Progress In Electromagnetics Research C, Vol. 95, 91–105, 2019

Experimental and Computational Analysis of the Effects of Tri-Band Antennas of Wearable Smart Glasses

Miraç D. Geyikoğlu[1], Fatih Kaburcuk[2], and Bülent Çavuşoğlu[1, *]

Abstract—The goal of this study is to analyze the effect of tri-band antennas in 2.45, 3.6, 3.8, 4.56, and 6 GHz frequencies, which cover Wi-Fi and some of the future 5G frequencies for wearable smart glasses applications. The latter 4 frequencies are studied for the first time for smart glasses. In order to provide a thorough analysis, first a simulation study for the head model with the proposed antennas is performed, then a realistic experiment by using a semi-liquid gel phantom head model with the infrared thermography method is conducted, and also 4 male subjects are included to analyze temperature rise effects on the skin. The phantom prepared for this study is also validated for its robustness and matching parameters. The SAR values and temperature rise due to the usage of smart glasses calculated by simulation modeling, bio-heat analytical solution, and infrared thermography technique are in good agreement. The temperature rise of the skin regions gets monotonically increased in the duration of usage. The simulations for all indicated frequencies are performed. Also, to provide comparable and practical results, the phantom study is compared with simulations for 2.45 GHz. According to the quantitative data obtained on the liquid-gel head phantom and on the subjects, the temperature increase is below 1°C, and its compliance with safety standards is determined. The results show that tri-band antennas for these frequencies can be safely used; however, a limiting behavior for the power is necessary for lower frequencies due to the increasing SAR values and temperature rise.

1. INTRODUCTION

Wearable wireless technologies (smart watches, smart glasses, etc.) have significant improvements in recent years. With the use of various wireless devices closer to the body, tissues absorb radiation from devices, and this radiation causes temperature rise. The interaction between tissues and wireless devices increases concerns about biological effects through increased use of wireless devices [1–3]. Especially for smart glasses, there have been technological advances and considerable studies in terms of their effects in recent years. When the studies for smart glasses are examined, effects of a mobile phone in terms of specific absorption rate (SAR) on the human head, with metallic [4–6] and plastic frame-glasses [7–11], are investigated. Cihangir et al. performed a study for effects of smart glasses with an integrated antenna operating at 4G and Wi-Fi communication on the human head in [7–11]. In their studies, SAR distribution on SAM and VH head phantom were analyzed, in which CE type antennas were placed in different areas of the head behind the ears. They used a SAM head phantom and a SAR measurement probe in their test measurements. The SAR distribution graph obtained according to the Wi-Fi frequency was also presented. With the development in the 5G technology, it is also important to investigate effects of an antenna, operating at 5G frequencies integrated into the smart glass model on the human head. Although the frequency range of the 5G does not have strictly defined frequency intervals, it is expected to be within the frequency ranges of 3.4–3.8 GHz, 4.4–4.9 GHz, 3.5–5.2 GHz,

Received 4 July 2019, Accepted 13 August 2019, Scheduled 1 September 2019
* Corresponding author: Bülent Çavuşoğlu (bcavusoglu@atauni.edu.tr).
[1] Electrical-Electronic Engineering Department, Ataturk University, Erzurum, Turkey. [2] Electrical and Electronic Engineering Department, Cumhuriyet University, Sivas, Turkey.

Table 1. Performance comparison of the different applications at 2.45 GHz.

Applications Type	**Description**	**SAR (W/kg)**
Eyewear Glasses [7–10]	CE type antenna, SAR measurement was performed using the SAR probe ($SAR_{10\,g}$), Power input: 0.25 W,	0.82
Wearable Antenna [1, 16, 17]	Microstrip antenna, SAR measurement was performed using the Infrared Thermography (Average SAR), Power input: 0.01 W	0.0013
Our study	Meandered dipole antenna, SAR measurement was performed using the Infrared Thermography (Average SAR), Power input: 0.02 W	0.0041

25.5–27 GHz, and 60–86 GHz [12–15]. Table 1 shows the smart glasses and wearable antennas studies in the literature. The methodologies and results of these studies are summarized in the table. As can be seen, the studies in the literature, to our knowledge, have not made an analysis for projected future 5G frequencies and their possible effects which are the main motivation of this study.

Electromagnetic simulation tools are generally used to investigate the interaction between an RF antenna and a human body for the safety assessment of RF antennas used in the wearable devices [1, 18, 19]. The SAR and thermal distributions on different human body parts at various frequencies are generally calculated using electromagnetic simulation tools (CST, HFSS etc.) These tools are insufficient in realizing complex structures of the body and in matching the realistic physical settings. Although the numerical modeling of microwave systems is ideally simulated, it does not give the realistic solutions due to non-ideal electrical, mechanical, and environmental factors [20]. Therefore, the presence of the human body is the best measurement environment for these systems. However, some experiments such as specific absorption rate (SAR) and hyperthermia are not suitable to be performed on a real human tissue when the power density and temperature rise in tissue are needed to be monitored [20]. Therefore, the use of artificial tissue phantoms is very useful for testing the microwave systems and temperature rise [21, 22]. In the literature, simplified tissue phantoms models such as homogeneous and multilayered models with straight, elliptical, rectangular sections are available [17]. For this study, a homogeneous and semi-liquid gel phantom is preferred. According to the literature studies about semi-liquid gel phantom, in order to increase the conductivity, salt is added to deionized water, while in order to reduce the permittivity of deionized water, some materials having low dielectric permittivity such as acrylic rod, polyethylene powder, polyvinyl chloride, polyoxyethylene, oil or sugar are added to deionized water [23–26]. Destruel et al., Simba et al. and Varshini et al. performed numerical and experimental research on SAR and power density from heat dynamics on an experimental phantom for the various resonance frequencies [1, 17, 27, 28].

Conventional SAR measurement systems are based on the electrical and magnetic field measurements and temperature distribution on the tissues [29–31]. In the literature, SAR values have been calculated accurately by using magnetic resonance thermal images and phantom thermal properties [32]. Varshini and Rama Rao proposed that the thermal distribution measurement using infrared thermography is a simple and effective technique that can be parallel to SAR or power density measurements to determine the suitability of wearable devices for various wireless applications or biocompatibility [17]. It is known that the effects of EM exposure on the biological tissues may cause temperature increase [16, 33]. In the last decades, important studies have been carried out for various frequencies. Several in-vivo and in-vitro studies have been conducted on thermal effects of RF exposure at variable densities and frequencies. According to these studies, RF exposure has some effects on neurotransmitter activities, immune system, brain tumors, cell motivation rates, etc. [2, 34]. Limited experimental studies have been reported to determine the real-time amount of temperature rise during the use of mobile telephones. The electromagnetic safety of the microwave systems which are in electromagnetic interaction with the human body is one of the important factors for technological developments.

In this study, the effects of different tri-band antennas integrated into smart glasses on a semi-liquid gel head phantom are investigated experimentally and numerically by using infrared thermography. The temperature rise on the skin is also quantitatively observed using smart glasses with 4 subjects at specific exposure times. This article attempts to focus on the biological effects of electromagnetic wave exposure on the human head. Additionally, the main objective of this study is to provide a quantitative measure of the SAR formed on the liquid phantom using smart glasses and temperature increase on the skin of human subjects which may be of immense importance considering the rapid growth in the use of smart glasses.

The paper is organized as follows. In Section 2, information about tri-band meandered dipole antennas and 3D wearable glasses is provided. In Section 3, a semi-liquid gel head phantom tissue model is prepared for proper electrical properties of the resonant frequencies of the antennas. In Section 4, using EM resources at the recommended power levels for operating frequencies, the SAR value and temperature change induced on the head phantom are analyzed by means of numerical modeling. Transient analysis based on temperature rise is obtained using 1-B bio heat equations. Temperature rises are investigated using the infrared thermography based on the duration of exposure of the EM waves to the body. In Section 5, temperature rise on the skin during the use of smart glasses of 4 subjects is examined. In Section 6, SAR values are calculated using thermal dynamic measurements and one-dimensional bio-heat transfer equations. Also, a comparative analysis is performed between the SAR values obtained by numerical modeling and thermal analysis.

2. THE EXPERIMENTAL SET-UP: ANTENNAS AND WEARABLE GLASSES MODEL

The direct contact of the antenna to the body causes a mismatch in the impedance of the antenna due to the dielectric load provided by the human tissues, thus alters the operating frequency of the antenna. Therefore, PLA (poly lactic acid) material with a high dielectric constant is preferred when designing wearable smart glasses in order not to affect the working frequency and reduce the effect of electromagnetic radiation on the head [35]. In order to place the antenna into 3D smart glasses, the right leg of the smart glasses model has a cavity whose dimension is $85 \times 25 \times 5\,\mathrm{mm}^3$. All dimensions of the smart glasses are given in Fig. 1. This study uses different meandered dipole antennas and wearable smart glasses model as shown in Fig. 2. The return loss (S_{11}) and bandwidth percentage values of prototype-1 and prototype-2 antennas are given in Fig. 3.

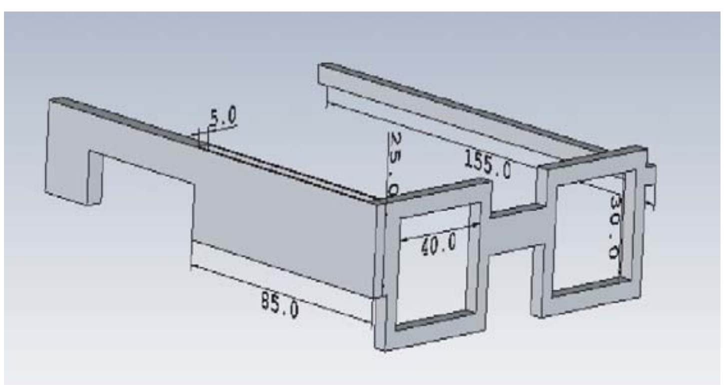

Figure 1. Illustration of the simulated 3D glasses.

3. PREPARING A SEMI-LIQUID PHANTOM FOR TISSUE MODELING

The dielectric properties of biological tissues are the determining factor for the distribution of electromagnetic energy in the human body. Therefore, relative permittivity, loss factor, and conductivity

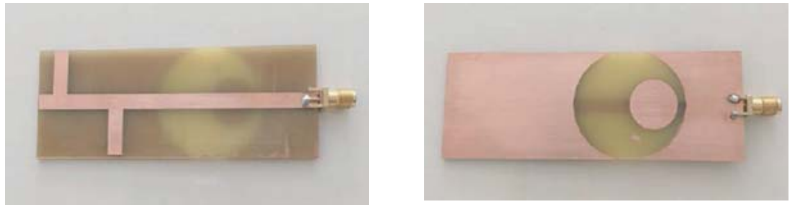

(a) Prototype-1 (left: top view, right: bottom view)

(b) Prototype-2 (left: top view, right: bottom view)

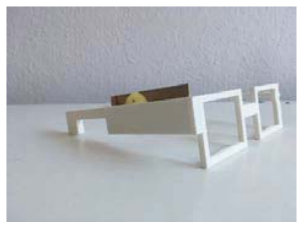

(c) 3D glasses manufactured

Figure 2. Pictures of (a) Prototype-1, (b) Prototype-2, (c) 3D glasses manufactured.

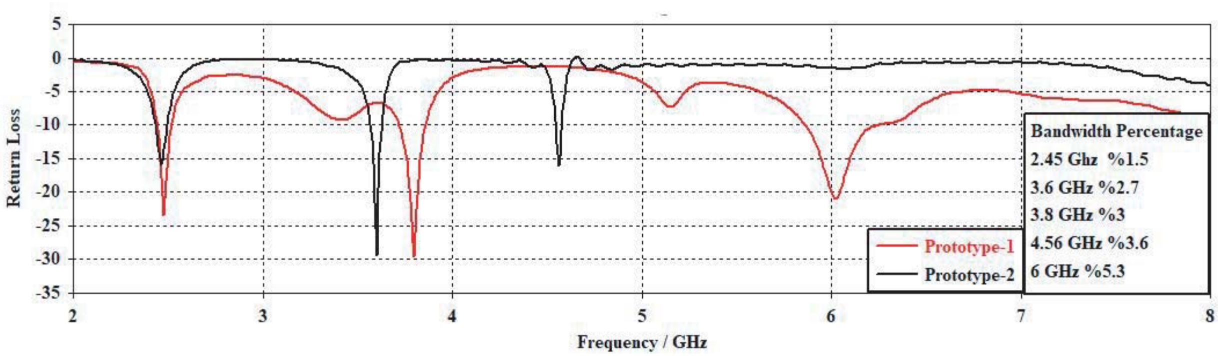

Figure 3. The S_{11} parameter of and the bandwidth percentage of the antennas for prototype-1 and prototype-2.

are important parameters for electromagnetic modeling and simulations. Although there have been many researchers who have measured the properties of various tissues of the body, in this study, the electrical properties of the tissues published by the Italian National Research Council at the interested resonance frequencies are adopted [36].

The electrical properties of the artificial tissue phantoms prepared for the examination of biological effects are very important for it to be comparable with real body tissues. The lifetime of the phantom is particularly important for the repeatability of the experiments and the continuation of the research. When selecting basic components of the phantom, low cost, water solubility, non-toxic and accessibility should be considered.

The human head is one of the most complex structures in the human body. It is not easy to simulate the human head because it includes many different tissues. The artificial tissue including homogenous material is used for the head phantom in many studies in order to facilitate the production

Table 2. The materials used to prepare semi-liquid head phantom.

Ingredients	SAM Head Phantom
Water (ml)	600
NaCl (g)	45
Sucrose (g)	1000
Gelatine (g)	2
Acidic organic liquid (ml)	5

process [23, 37].

In this study, the required protocol in the preparation of semi-liquid gel phantom to be used for the SAM head model is given below. The quantity of materials used for the phantom is given in Table 2.

- The mixture is stirred until the solution is dissolved and heated up to 100°C. After heating, the mixture is stirred again with the mixer until it falls to the room temperature.
- After the phantom reaches room temperature, the mixture is rested until the air bubbles are minimized. The materials used and the properties they affect are given below.
- Solvent: deionized water.
- Conductivity control: sodium chloride (NaCI).
- Permeability control: sucrose (table sugar).
- Protector: acidic organic liquid.
- Gelling agent: Gelatine.

Phantom measurements have been carried out using the Keysight FieldFox N9928A vector network analyzer with 30 kHz–26.5 GHz frequency range and Keysight 85070E slim form coaxial probe operating between 50 MHz and 50 GHz. The experimental setup to measure the dielectric properties of the prepared phantom is shown in Fig. 4.

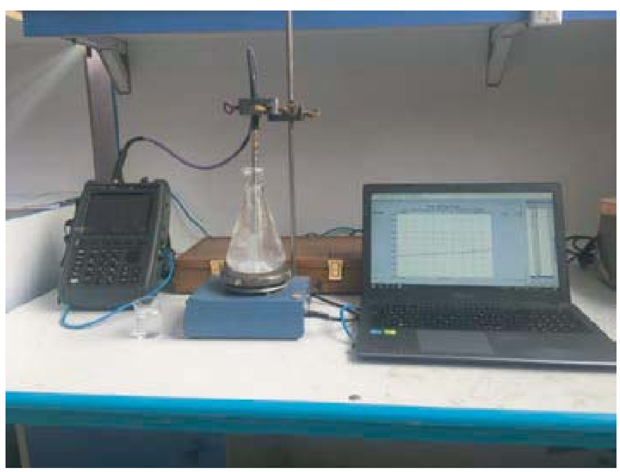

Figure 4. The experimental setup essential for measuring the electrical properties of the prepared phantom.

The complex relative permittivity of the phantom is measured by the Keysight 85070E software. According to the complex relative permittivity Equation (1) [38], the dielectric constant ε_r' and loss tangent value $\varepsilon_r'/\varepsilon_r''$ are calculated. Using these two values in Equation (2) [38], the conductivity of the tissue is calculated.

$$\varepsilon_c = \varepsilon_r' - j\varepsilon_r'' = \varepsilon_r = -j\varepsilon_r \tan\delta \tag{1}$$

$$\sigma = w\varepsilon_o\varepsilon_o\varepsilon_r \tan\delta \quad (2)$$

When the dielectric properties of the prepared SAM head phantom are compared to those obtained in [39], it is observed that the parameters are within the $+-10\%$ difference range. The dielectric properties of the prepared phantom have been measured in 24 hour intervals for 2 weeks at room temperature. According to the obtained data, the change in the dielectric properties of the phantom is found to be around 3% which is quite stable. The graph of the obtained data is shown in Fig. 5.

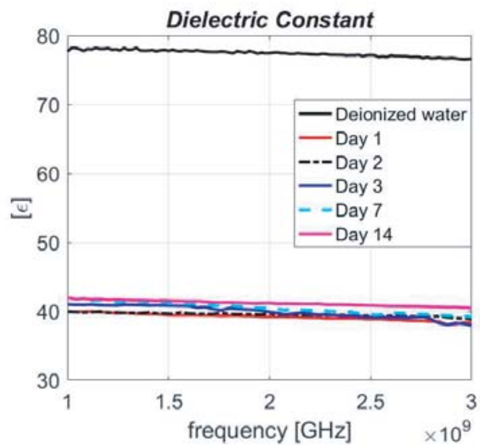

Figure 5. The measured dielectric constant of the semi-liquid phantom within two-week period.

4. EVALUATION OF THE EFFECTS OF 5G ANTENNAS DESIGNED FOR WEARABLE GLASSES ON SEMI-LIQUID HEAD PHANTOM

In order to obtain the SAR value and temperature changes on the biological tissues due to the radiation from the wearable wireless devices, numerical analysis and transient temperature analysis have been performed. In order to evaluate simulation results, the prepared semi-liquid gel phantom wearing the smart glasses model including an antenna is used to measure the thermal distribution using infrared thermography.

4.1. SAR and Temperature Simulation for Resonance Frequencies

The limits of SAR values, the electromagnetic energy absorbed by biological tissues, are determined by international standards [40]. According to these standards, the average of SAR must be 1.6 W/kg over any 1 gram of tissue ($SAR_{1\,g}$) and 2 W/kg over any 10 gram of tissue ($SAR_{10\,g}$). The input power of the mobile devices can be adjusted to an appropriate level for limiting the SAR. It is well known that the SAR values depend on the frequency of interest, antenna types, and distance between the human head and antenna. In this study, SAR values on the human head with and without 3D smart glasses are calculated when the input power of the antenna is set to 20 mW. SAM head phantom provided in the library of CST Microwave Studio Suite is used as a human head model. The dielectric properties of the SAM head phantom at the frequencies of interest are given in Table 3. The SAM phantom wearing the smart glasses model with the embedded antenna in the CST simulation environment is shown in Fig. 6.

The average SAR values for two tri-band antennas (named as prototype-1 and prototype-2) are obtained for the SAM head phantom with and without the smart glasses, given in Table 4. It can be seen from Table 4 that average SAR values obtained for prototype-2 at the frequencies of interest are higher than that for prototype-1. The efficiency of prototype-2 antenna is higher than that of prototype-1 antenna. Hence, the higher SAR values for prototype-2 are already expected due to its higher efficiency. The SAR and temperature values obtained from the simulation results are given in Table 4.

Table 3. The dielectric and thermal properties of the SAM head phantom at the frequencies [39].

Frequency (GHz)	Permittivity (F/m)	Elec. Cond. (S/m)	Loss tangent ($\tan\delta$)	Density (kg/m^3)	Therm. Cond (W/m/K)	Heat Capacity (J/kg/K)
2.45	39.2	1.8	0.336	1046	51	3630
3.6	37.95	3.1	0.407			
3.8	37.6	3.23	0.406			
4.56	36.2	3.94	0.429			
6	35.1	5.48	0.467			

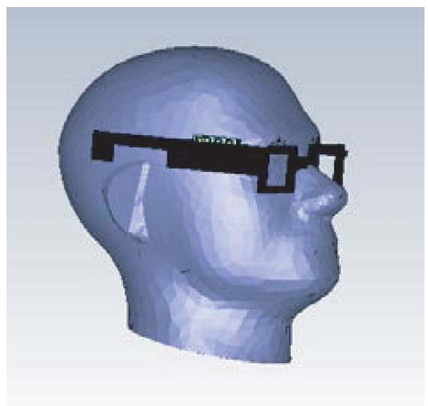

Figure 6. The simulated glasses and SAM phantom view in CST simulation environment.

Table 4. Simulated SAR (10^{-2} W/kg) and temperature (°C) values using SAM head phantom.

Prototype	Frequency (GHz)	Local Average SAR (10^{-2} W/kg)		Local Temperature (°C)	
		13 dBm (without glasses)	13 dBm (with glasses)	13 dBm (without glasses)	13 dBm (with glasses)
1	2.45	4.102	2.024	18.25	20.05
	3.8	3.437	1.853	18.15	19.8
	6	2.962	1.456	17.75	18.75
2	2.45	4.24	2.974	21.5	21.47
	3.6	3.87	2.42	21.1	21.25
	4.56	3.51	1.92	20.8	20.75

4.2. Transient and Numerical Analysis of Temperature Variation

Transient analysis of the temperature increase in the time domain is one of the important issues. There are two different approaches depending on whether the thickness of the tissue in the body region is smaller or larger than the wavelength considered. Because the tissue thickness is greater than the wavelength in this study, Equation (3) [41] is used. This equation is the 1D bio heat equation, written according to the Fourier series

$$T\left(t\right)=\frac{q}{2\lambda^{\iota}}\frac{\sqrt{\lambda}^{\iota}A}{r}\left\{\begin{array}{c}\dfrac{e^{r-\sqrt{\lambda}^{\iota}A}}{2}\left(1+\dfrac{1}{\sqrt{\lambda}^{\iota}A}\right)\cdot erfc\left(\dfrac{r-\sqrt{\lambda}^{\iota}A}{2\sqrt{\tau}}\right)\\ +\frac{e^{-(r-\sqrt{\lambda}^{\iota}A)}}{2}\left(1-\frac{1}{\sqrt{\lambda}^{\iota}A}\right)\cdot erfc\left(\frac{r-\sqrt{\lambda}^{\iota}A}{2\sqrt{\tau}}-\sqrt{\tau}\right)\\ +\dfrac{e^{\left(r+\sqrt{\lambda}^{\iota}A\right)}}{2}\left(1-\dfrac{1}{\sqrt{\lambda}^{\iota}A}\right)\cdot erfc\left(\dfrac{r+\sqrt{\lambda}^{\iota}A}{2\sqrt{\tau}}+\sqrt{\tau}\right)\\ +\dfrac{e^{-\left(r+\sqrt{\lambda}^{\iota}A\right)}}{2}\left(1+\dfrac{1}{\sqrt{\lambda}^{\iota}A}\right)\cdot erfc\left(\dfrac{r+\sqrt{\lambda}^{\iota}A}{2\sqrt{\tau}}-\sqrt{\tau}\right)\\ +\dfrac{r}{\sqrt{\lambda}^{\iota}A}e^{-\tau}\left[erfc\left(\dfrac{r+\sqrt{\lambda}^{\iota}A}{2\sqrt{\tau}}\right)-erfc\left(\dfrac{r-\sqrt{\lambda}^{\iota}A}{2\sqrt{\tau}}\right)\right.\\ \left.+\dfrac{2}{\sqrt{\lambda}^{\iota}A}\sqrt{\dfrac{\tau}{\Pi}}(\exp-\dfrac{\left(r-\sqrt{\lambda}^{\iota}A\right)^{2}}{4\tau}-\exp-\dfrac{\left(r+\sqrt{\lambda}^{\iota}A\right)^{2}}{4\tau})\right]\end{array}\right\}\tag{3}$$

where $\tau=\frac{\lambda^{\iota}}{\mu}t$; $r=\sqrt{\lambda}^{\iota}R$; $\mu=\frac{\rho c}{K}$; $erfc(x)=1-\frac{2}{\sqrt{\Pi}}\int_{0}^{x}e^{-t^{2}}dt$; $q=\frac{\rho\cdot S}{K}$; $\lambda^{\iota}=\frac{\rho_{b}c_{b}\rho w}{\sigma}$. q is equal to mass density multiplied by the average SAR value and divided by the thermal conductivity; μ is equal to density multiplied by the heat capacity and divided by the thermal conductivity of tissue; S is the average SAR (w/kg); ρ is the mass density of tissue (kg/m^3); K is the thermal conductivity of the tissues (w/m/K); ρ_b is the mass density of tissue (kg/m^3); C is the heat capacity of the tissue (J/kg/K); c_b is the heat capacity of the blood (J/kg/K); ω is the blood perfusion rate ((ml/g/s); λ is the wavelength of the EM wave (m); R is the tissue thickness (m); A is lambda (in meters) divided by 4; $erfc(x)$ is the error function.

Transient temperature analysis of the tri-band antennas is performed for the case where the antenna excited by the input power of 13 dBm is imposed with and without glasses on the phantom.

Temperature changes have been calculated by implementing Eq. (3) in Matlab for specific exposure times and various operation frequencies, and the results are shown in Fig. 7. The decrease in wavelength due to the increase in frequency leads to lower temperature rise at the same exposure times.

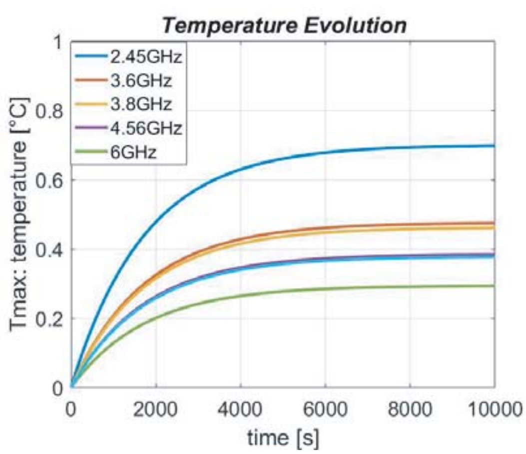

Figure 7. The graph of changes in temperature values according to the exposure time.

4.3. Temperature Analysis with Infrared Thermography Method

Infrared thermography is a non-contact temperature measurement technique where infrared rays emitted from the surface of an object are detected using a suitable infrared detector, and the temperature of the object is measured by the radiated radiation intensity. Thermography data are obtained using the radiometric equation (Eq. (4)) [2]

$$R_{cam} = T\varepsilon R_{obj} + T\,(1-\varepsilon)\,R_{env} + (1-T)R_{atm} \tag{4}$$

R_{cam} is the radiance received by the infrared detector placed inside the camera; R_{obj}, R_{env}, R_{atm} show the radiation emitted by the object under investigation, surrounding environment, and the atmosphere, respectively; T and ε are the atmospheric transmittance and emissivity of the surface of the object under investigation, respectively. The radiance received by the infrared detector is converted to an electrical signal, and the object temperature is measured using appropriate calibration curves.

Infrared Thermography method captures the temperature distribution on the surface and presents it as visible information. Analysis is performed only for 2.45 GHz frequencies due to equipment limitations (our frequency generator Hameg Instruments 8135 can go only up to 3 GHz). Infrared thermography analysis of wearable glasses has not been performed in earlier studies. Through this analysis it also aims to calculate the SAR values and compare it with the simulations. The test environment prepared for measuring the thermal dynamics on the phantom when being exposed to the RF output of the tri-band antenna is shown in Fig. 8. The antenna placed on the phantom in a dark non-reflective environment is

Figure 8. The experimental setup for infrared thermography. a) Signal generator, c) vector network analyzer, e) inside of the dark box, b) infrared camera, d) semi-liquid gel phantom and eyewear glasses.

Table 5. SAR (10^{-2} W/kg) and temperature (°C) results obtained from infrared thermography experimental results in 2.45 GHz.

Frequency (2.45 GHz)		600 (s)		1200 (s)		1800 (s)	
		13 dBm (without glasses)	13 dBm (with glasses)	13 dBm (without glasses)	13 dBm (with glasses)	13 dBm (without glasses)	13 dBm (with glasses)
Prototype-1	SAR (10^{-2} W/kg)	1.21	0.605	1.21	0.605	1.613	0.806
	Temp. Rise (°C)	0.2	0.1	0.2	0.1	0.3	0.2
Prototype-2	SAR (10^{-2} W/kg)	1.21	1.21	1.5125	0.9075	1.41	0.806
	Temp. Rise (°C)	0.2	0.2	0.3	0.1	0.2	0.1

fed through a signal generator. Thermograms are obtained for the exposure times of 10, 20, 30 minutes where the antennas with and without glasses are placed on the phantom (Fig. 9). The color scale given on the right in Fig. 8 changes according to the automatic calibration of the thermal imager in the images. The temperature value given in the upper left corner shows the instantaneous average value of the setting. Temperature increase information for different durations is presented in Table 5. SAR evaluation can be performed using the temperature data obtained from thermal images and Eq. (5) [40].

$$SAR = c\frac{\Delta T}{\Delta t} \tag{5}$$

where c (J/kg/°C) is the tissue heat capacity, T (°C) the temperature, and t (s) the time.

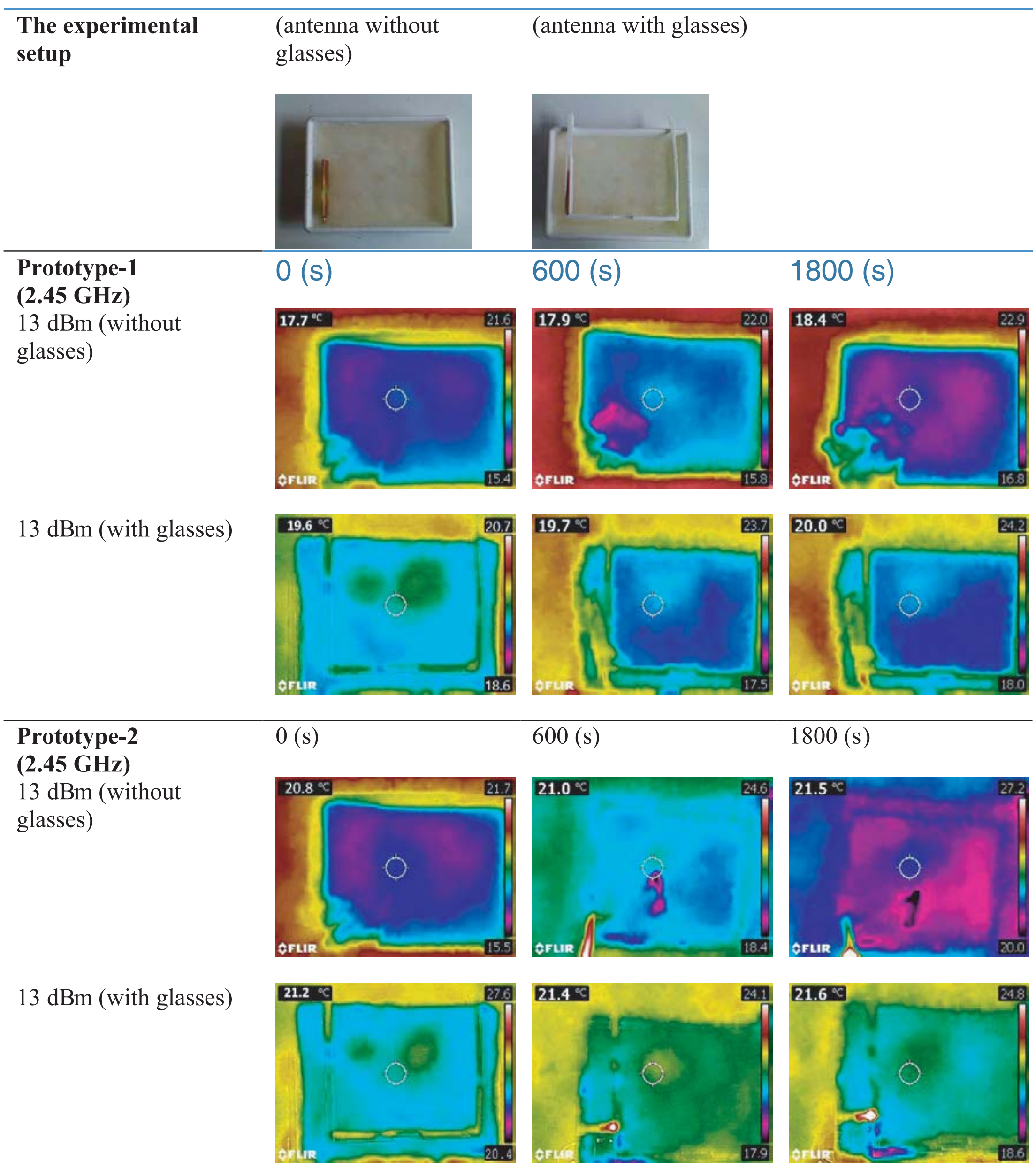

Figure 9. Thermogram images of the antennas according and corresponding exposure times, with glasses and without glasses in a semi-liquid gel phantom.

5. EVALUATION OF THE EFFECTS OF 5G ANTENNAS DESIGNED FOR WEARABLE GLASSES ON HEAD SKIN

Considering the use of rapidly spreading electronic devices, quantitative measurements of temperature changes that may occur in the front or side profile of the head during the use of smart glasses are presented in this study. Experiments are performed on four healthy adult subjects (four males) in the 24–26 age group. The height and weight of the subjects are ranged 150–172 cm and 65–85 kg, respectively. The thermogram samples obtained by placing prototype-1 antenna on the user's head with the 3D glasses model are given in Fig. 10. The temperature rise that occurs according to the thermogram results obtained from the subjects is presented in Table 6. According to the results, it is thought that the temperature variations between the subjects are due to differences in the electrical properties between the tissues related to the structure of the person and the water ratios of their bodies.

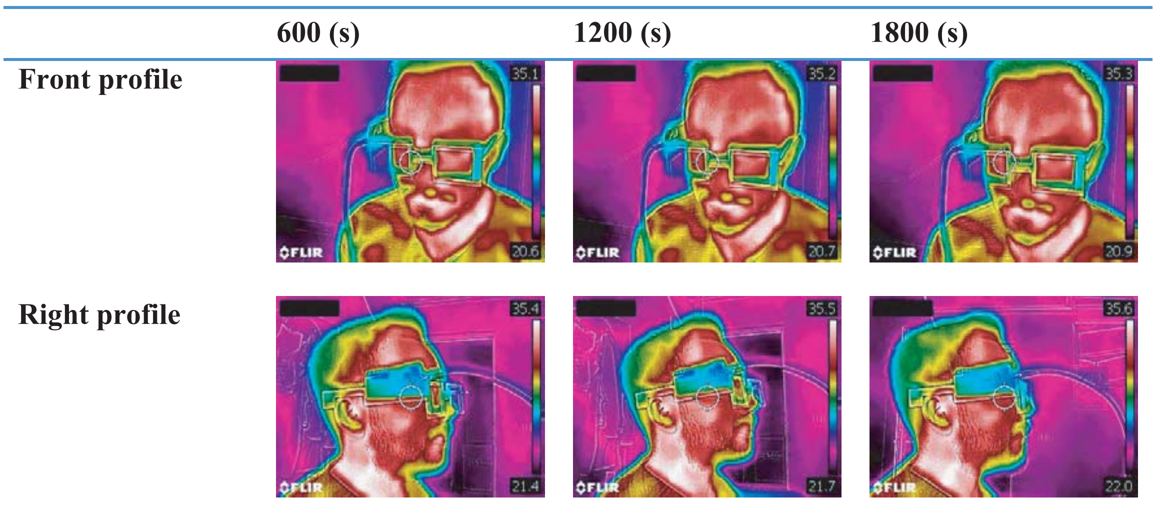

Figure 10. Thermogram images of the Prototype-1 (2.45 GHz) antenna based on the exposure time of with glasses on head skin.

Table 6. The temperature increase of the front and right profile regions results obtained from infrared thermography experimental results (2.45 GHz).

		Exposure Time		
		600 (s)	1200 (s)	1800 (s)
		Temperature rise (°C)		
Prototype-1	Subject 1	0.1	0.1	0.1
	Subject 2	0.1	0.2	0.1
	Subject 3	0.1	0.2	0.3
	Subject 4	0.1	0.2	0.2
Prototype-2	Subject 1	0.1	0.1	0.2
	Subject 2	0.1	0.2	0.2
	Subject 3	0.1	0.1	0.2
	Subject 4	0.1	0.2	0.3

6. COMPARISON OF THERMAL EFFECTS AND SAR VALUE ON SEMI-LIQUID PHANTOM BY NUMERICAL, TRANSIENT ANALYSIS, AND EXPERIMENTAL METHODS

Temperature and SAR values comparisons of the results between the simulation modeling and transient temperature analysis, and infrared thermography methods are shown in Fig. 11.

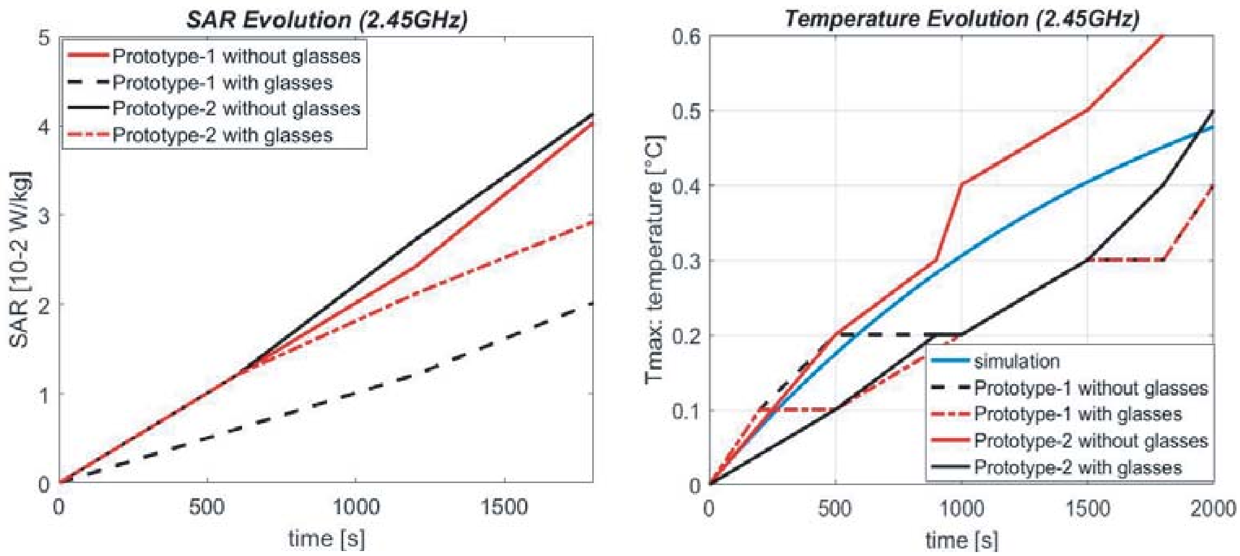

Figure 11. Comparison of SAR and temperature values for the transient temperature analysis and infrared thermography methods.

According to the temperature values obtained from thermography results, the increase in temperature caused by Prototype-1 is closer to the numerical results obtained by transient temperature analysis, while the increase in temperature caused by Prototype-2 is measured higher than the transient temperature analysis values. It is thought that this may be due to the difference in the efficiency of the antennas or environmental factors. When temperature changes are compared with or without glasses, low-temperature changes are observed due to the effect of glasses.

The SAR values for Prototype-1 and Prototype-2 are calculated based on the temperature rise on the phantom for both cases, "with glasses" and "without glasses". Due to the limitation of the infrared camera sensitivity, the minimum increase is measured in steps of 0.1°C. Therefore, the calculated SAR values are approximate values.

7. CONCLUSION

This study reports the bio-electromagnetic effect of triband meandered dipole antennas resonating at 2.45, 3.6, 3.8, 4.56, and 6 GHz when being used for wearable smart eyeglasses.

The antenna effects on biological tissues are examined for both with and without glasses cases on the SAM head model in terms of SAR values and thermal effects for several exposure time durations. Due to the decrease in permittivity at high frequencies, it is observed that the effect on biological tissues decreases with increasing resonance frequency. This results in less absorption, less SAR, and less thermal effect in the tissues.

Numerical analysis is performed according to electrical and thermal properties of the respective tissues and exposure times by using 1-B Penne heat equation. A semi-liquid gel phantom having electrical properties of the respective frequencies is prepared to examine the temperature increase of the tissues due to RF exposure by analytical and infrared thermography technique. Temperature analysis is performed according to various exposure times in infrared thermography technique. SAR values are calculated by using numerical analysis from the obtained temperature values.

The temperature rise on the skin is determined quantitatively by infrared thermography technique on 4 human subjects with similar age groups.

In this study, simulation modeling, numerical analysis, and experimental infrared thermography methods are used to compare the maximum temperature increase at various frequencies. According to the quantitative data obtained on the liquid-gel head phantom prepared and on the subjects, the temperature increase stay below 1°C, and its compliance with the safety standards is observed. Hence, it can be deduced from the results that the tri-band antennas which are the subject of this study can be safely used and embedded in the glasses for analyzed frequencies. This study also helps to understand positive effects of the frame of glasses in terms of thermal and SAR effects since the frames take the role of a protective shield for the head.

REFERENCES

1. Varshini, K. and T. Rama Rao, "Estimation of specific absorption rate using infrared thermography for the biocompatibility of wearable wireless devices," *Progress In Electromagnetics Research M*, Vol. 56, 101–109, 2017.
2. Lahiri, B., S. Bagavathiappan, C. Soumya, T. Jayakumar, and J. Philip, "Infrared thermography based studies on mobile phone induced heating," *Infrared Physics & Technology*, Vol. 71, 242–251, 2015.
3. Repacholi, M. H., "Low-level exposure to radiofrequency electromagnetic fields: Health effects and research needs," *Bioelectromagnetics: Journal of the Bioelectromagnetics Society, the Society for Physical Regulation in Biology and Medicine, the European Bioelectromagnetics Association*, Vol. 19, No. 1, 1–19, 1998.
4. Zhang, M. and X. Wang, "Influence on SAR due to metallic frame of glasses based on high-resolution Chinese electromagnetic human model," *2010 Asia-Pacific Symposium on Electromagnetic Compatibility (APEMC)*, 48–51, IEEE, 2010.
5. Pizarro, Y., A. De Salles, S. Severo, J. Garzón, and S. Bueno, "Specific Absorption Rate (SAR) in the head of Google glasses and Bluetooth user's," *2014 IEEE Latin-America Conference on Communications (LATINCOM)*, 1–6, IEEE, 2014.
6. Bellanca, G., G. Caniato, A. Giovannelli, P. Olivo, S. J. M. Trillo, and O. T. Letters, "Effect of field enhancement due to the coupling between a cellular phone and metallic eyeglasses," *Microwave & Optical Technology Letters*, Vol. 48, No. 1, 63–65, 2006.
7. Cihangir, A., et al., "Dual-band 4G eyewear antenna and SAR implications," *IEEE Transactions on Antennas and Propagation*, Vol. 65, No. 4, 2085–2089, 2017.
8. Cihangir, A., C. J. Panagamuwa, W. G. Whittow, F. Gianesello, C. J. I. A. Luxey, and W. P. Letters, "Ultra-broadband antenna with robustness to body detuning for 4G eyewear devices," *IEEE Antennas and Wireless Propagation Letters*, Vol. 16, 1225–1228, 2017.
9. Cihangir, A., W. Whittow, C. Panagamuwa, G. Jacquemod, F. Gianesello, and C. J. C. R. P. Luxey, "4G antennas for wireless eyewear devices and related SAR," *Comptes Rendus Physique*, Vol. 16, No. 9, 836–850, 2015.
10. Cihangir, A., et al., "Feasibility study of 4G cellular antennas for eyewear communicating devices," *IEEE Antennas and Wireless Propagation Letters*, Vol. 12, 1704–1707, 2013.
11. Lan, J., X. Liang, T. Hong, G. J. P. I. b. Du, and M. Biology, "On the effects of glasses on the SAR in human head resulting from wireless eyewear devices at phone call state," *Progress in Biophysics and Molecular Biology*, Vol. 136, 29–36, August 2018.
12. Tikhomirov, A., E. Omelyanchuk, and A. Semenova, "Recommended 5G frequency bands evaluation," *2018 Systems of Signals Generating and Processing in the Field of on Board Communications*, 2018.
13. Letavin, D. A. and D. A. Trifonov, "Simulation of 3600–3800 MHz frequency band antenna for fifth generation mobile communication," *2018 Ural Symposium on Biomedical Engineering, Radioelectronics and Information Technology (USBEREIT)*, 291–294, IEEE, 2018.

14. Qamar, F., M. H. S. Siddiqui, K. Dimyati, K. A. B. Noordin, and M. B. Majed, "Channel characterization of 28 and 38 GHz MM-wave frequency band spectrum for the future 5G network," *2017 IEEE 15th Student Conference on Research and Development (SCOReD)*, 291–296, IEEE, 2017.
15. Pandit, S., A. Mohan, and P. J. I. S. L. Ray, "Compact frequency-reconfigurable MIMO antenna for microwave sensing applications in WLAN and WiMAX frequency bands," *IEEE Sensors Letters*, Vol. 2, No. 2, 1–4, 2018.
16. Karthik, V. and T. R. Rao, "Investigations on SAR and thermal effects of a body wearable microstrip antenna," *Wireless Personal Communications*, Vol. 96, No. 3, 3385–3401, 2017.
17. Varshini, K. and T. Rama Rao, "Thermal distribution based investigations on electromagnetic interactions with the human body for wearable wireless devices," *Progress In Electromagnetics Research M*, Vol. 50, 141–150, 2016.
18. Brishoual, M., C. Dale, J. Wiart, and J. Citerne, "Methodology to interpolate and extrapolate SAR measurements in a volume in dosimetric experiment," *IEEE Transactions on Electromagnetic Compatibility*, Vol. 43, No. 3, 382–389, 2001.
19. Chavannes, N., R. Tay, N. Nikoloski, and N. Kuster, "RF design of mobile phones by TCAD: Suitability and limitations of FDTD," *IEEE Antennas Propagation Mag.*, Vol. 45, 52–66, 2003.
20. Mobashsher, A. T. and A. M. Abbosh, "Artificial human phantoms: Human proxy in testing microwave apparatuses that have electromagnetic interaction with the human body," *IEEE Microwave Magazine*, Vol. 16, No. 6, 42–62, 2015.
21. Bakar, A. A., A. Abbosh, P. Sharpe, and M. Bialkowski, "Artificial breast phantom for microwave imaging modality," *2010 IEEE EMBS Conference on Biomedical Engineering and Sciences (IECBES)*, 385–388, IEEE, 2010.
22. Islam, M. T., M. Samsuzzaman, S. Kibria, and M. T. Islam, "Experimental breast phantoms for estimation of breast tumor using microwave imaging systems," *IEEE Access*, Vol. 6, 78587–78597, 2018.
23. Duan, Q., et al., "Characterization of a dielectric phantom for high-field magnetic resonance imaging applications," *Medical Physics*, Vol. 41, No. 10, 102303, 2014.
24. Soler González, F., "Radiation effects of wearable antenna in human body tissues," EEE *Student Reports (FYP/IA/PA/PI)*, 2014.
25. Castelló-Palacios, S., C. Garcia-Pardo, A. Fornes-Leal, N. Cardona, and A. Vallés-Lluch, "Wideband phantoms of different body tissues for heterogeneous models in body area networks," *2017 39th Annual International Conference of the IEEE Engineering in Medicine and Biology Society (EMBC)*, 3032–3035, IEEE, 2017.
26. Castelló-Palacios, S., C. Garcia-Pardo, A. Fornes-Leal, N. Cardona, and A. Vallés-Lluch, "Tailor-made tissue phantoms based on acetonitrile solutions for microwave applications up to 18 GHz," *IEEE Transactions on Microwave Theory and Techniques*, Vol. 64, No. 11, 3987–3994, 2016.
27. Destruel, A., et al., "A numerical and experimental study of RF shimming in the presence of hip prostheses using adaptive SAR at 3 T," *Magnetic Resonance in Medicine*, 2019.
28. Simba, A., S. Watanabe, T. Hikage, and T. Nojima, "Experimental and numerical investigation of the maximum specific absorption rate in a spherical phantom when operating a mobile phone near a metallic wall," *IET Science, Measurement & Technology*, Vol. 5, No. 6, 225–230, 2011.
29. Abdelsamie, M. A., S. Mustafa, M. Isa, and D. Hashim, "Evaluation of electric and magnetic fields distribution and SAR induced in 3D models of water containers by radiofrequency radiation and their relationship to the non-thermal effects of microwaves," arXiv preprint arXiv:1410.2147, 2014.
30. Wessapan, T., S. Srisawatdhisukul, and P. Rattanadecho, "Specific absorption rate and temperature distributions in human head subjected to mobile phone radiation at different frequencies," *International Journal of Heat and Mass Transfer*, Vol. 55, No. 1–3, 347–359, 2012.
31. Hamada, L., T. Iyama, T. Onishi, and S. Watanabe, "The specific absorption rate of mobile phones measured in a flat phantom and in the standardized human head phantom," *EMC09 21S4-1*, 245–247, 2009.

32. Alon, L., D. K. Sodickson, and C. M. Deniz, "Heat equation inversion framework for average SAR calculation from magnetic resonance thermal imaging," *Bioelectromagnetics*, Vol. 37, No. 7, 493–503, 2016.
33. Foster, K. R., "Thermal and nonthermal mechanisms of interaction of radio-frequency energy with biological systems," *IEEE Transactions on Plasma Science*, Vol. 28, No. 1, 15–23, 2000.
34. Sarimov, R., L. O. Malmgren, E. Marková, B. R. Persson, and I. Y. Belyaev, "Nonthermal GSM microwaves affect chromatin conformation in human lymphocytes similar to heat shock," *IEEE Transactions on Plasma Science*, Vol. 32, No. 4, 1600–1608, 2004.
35. Huber, E., M. Mirzaee, J. Bjorgaard, M. Hoyack, S. Noghanian, and I. Chang, "Dielectric property measurement of PLA," *2016 IEEE International Conference on Electro Information Technology (EIT)*, 0788–0792, IEEE, 2016.
36. https://www.omicsonline.org/universities/Italian_National_Research_Council/.
37. La Gioia, A., et al., "Open-ended coaxial probe technique for dielectric measurement of biological tissues: Challenges and common practices," *Diagnostics*, Vol. 8, No. 2, 40, 2018.
38. Zajícek, R. and J. Vrba, "Broadband complex permittivity determination for biomedical applications," *Advanced Microwave Circuits and Systems*, 365–385, IntechOpen, 2010.
39. https://speag.swiss/products/em-phantoms/phantoms/sam-v4-5bs/.
40. I. S. C. C. 34, "IEEE recommended practice for determining the peak spatial-average Specific Absorption Rate (SAR) in the human head from wireless communications devices: Measurement techniques," *Standard 1528-2003*, Institute of Electrical and Electronic Engineers, 2003.
41. Kritikos, H. and H. P. Schwan, "Potential temperature rise induced by electromagnetic field in brain tissues," *IEEE Transactions on Biomedical Engineering*, Vol. 26, No. 1, 29–34, 1979.